AIAA JOURNAL
Vol. 47, No. 9, September 2009

Technical Notes

Pressurized Hollow Spherical Vessels with Arbitrary Radial Nonhomogeneity

X.-F. Li,* X.-L. Peng, and Y.-A. Kang
Central South University,
410083 Changsha, People's Republic of China

DOI: 10.2514/1.41995

Nomenclature

A	=	constant of integration
a	=	inner radius
B	=	constant of integration
b	=	outer radius
c_m	=	constant coefficients
E, $E(r)$, $E^*(r)$	=	Young's modulus (dependent on r)
E_i	=	Young's modulus at the inner surface
$F(r,t)$	=	kernel of normalized Fredholm integral equation
$f(r)$	=	known function defined by Eq. (10)
$K(r,t)$	=	kernel of Fredholm integral equation
$L(r,t)$	=	kernel of Fredholm integral equation
$P_n(x)$	=	Legendre polynomials
q_i, q_o	=	pressure at the inner and outer surfaces
r	=	radial coordinate
t	=	normalized radial variable
u_r	=	radial displacement
x	=	normalized radial variable
α	=	ratio of Young's modulus at the outer surface to that at the inner surface
β	=	gradient index
θ	=	polar angle coordinate
ν, $\nu(r)$	=	Poisson's ratio (dependent on r)
σ_r	=	radial stress
σ_θ	=	circumferential stress
φ	=	azimuth-angle coordinate

I. Introduction

SPHERICAL vessels are widely used in engineering applications. The stress distribution of pressurized spherical vessels is very significant for better understanding of their mechanical behavior. Such topics have attracted considerable attention of researchers.

For a homogeneous hollow sphere, a closed-form solution under uniform pressure has been obtained for various cases [1]. For spherically symmetrical problems of a multilayered hollow sphere subjected to internal or external pressure, analytical methods have been proposed to derive its explicit expressions for stresses [2–4]. Because of the mismatch of material properties at the interface, the hoop stress has a jump at the interface, which might yield failure of structure. Such a drawback can be obviated when multilayered structures are replaced by functionally graded materials (FGMs) [5], and so the occurrence of failure of pressurized spherical vessels can be lowered. For FGM hollow spheres or cylinders, great progress has been made for specified gradients such as power-law and exponential forms [6–10]. By requiring constant shear stress or constant hoop stress in a pressurized FGM hollow sphere, an approach of optimal design of a pressurized FGM hollow vessel has been given in [11,12].

Most of the aforementioned works focus on a power-law gradient or exponential gradient, and the obtained results fail to apply to arbitrarily varying gradients. This Note presents a new analytical approach to determine the elastic field of an FGM hollow spherical vessel with spherical isotropy and spherically transversely isotropy. The material properties of the spherical shell may arbitrarily vary as continuous or piecewise functions. The elastic problem to be solved is reduced to an integral equation. By numerically solving the resulting equation, the stress distribution can be determined. Numerical results are presented graphically to show the effects of the gradient on the radial and hoop stresses.

II. Theoretical Formulation

Consider a spherically symmetrical problem made of FGMs. Adopting a spherical coordinate system (r, θ, and φ), the basic stress–strain relations are

$$\frac{\mathrm{d}u_r}{\mathrm{d}r} = \frac{1}{E}(\sigma_r - 2\nu\sigma_\theta), \qquad \frac{u_r}{r} = \frac{1}{E}[(1-\nu)\sigma_\theta - \nu\sigma_r] \tag{1}$$

In the absence of body forces, the following equilibrium equation should be satisfied:

$$\frac{\mathrm{d}\sigma_r}{\mathrm{d}r} + \frac{2(\sigma_r - \sigma_\theta)}{r} = 0 \tag{2}$$

In this Note, Young's modulus and Poisson's ratio are assumed to be dependent on r [i.e., $E = E(r)$ and $\nu = \nu(r)$]. To obtain σ_r and σ_θ, we first express them in terms of u_r:

$$\sigma_r = \frac{E(r)}{[1+\nu(r)][1-2\nu(r)]}\left[(1-\nu(r))\frac{\mathrm{d}u_r}{\mathrm{d}r} + 2\nu(r)\frac{u_r}{r}\right] \tag{3}$$

$$\sigma_\theta = \frac{E(r)}{[1+\nu(r)][1-2\nu(r)]}\left[\frac{u_r}{r} + \nu(r)\frac{\mathrm{d}u_r}{\mathrm{d}r}\right] \tag{4}$$

From Eq. (3), we can get

$$u_r = \frac{1}{\chi(r)}\left[A + \int_{r_0}^{r} \frac{[1+\nu(s)][1-2\nu(s)]\chi(s)}{[1-\nu(s)]E(s)}\sigma_r(s)\,\mathrm{d}s\right] \tag{5}$$

where r_0 is a parameter, A is a constant to be determined through proper boundary conditions, and $\chi(r)$ is defined by

$$\chi(r) = \exp\left[\int_{r_0}^{r} \frac{2\nu(s)}{[1-\nu(s)]s}\,\mathrm{d}s\right] \tag{6}$$

In addition, from Eqs. (3) and (4), we get

$$\sigma_\theta = \frac{\nu(r)}{1-\nu(r)}\sigma_r + \frac{E(r)}{1-\nu(r)}\frac{u_r}{r} \tag{7}$$

Thus, once σ_r is determined, u_r and σ_θ can be obtained by Eqs. (5) and (7), respectively. Clearly, u_r is always continuous, even for piecewise-continuous $E(r)$ and $\nu(r)$. However, this is not true for σ_θ, because it has a jump at the interface due to the mismatch of $E(r)$ and

Received 4 November 2008; revision received 8 April 2009; accepted for publication 21 May 2009.

*Institute of Mechanics and Sensor Technology, School of Civil Engineering and Architecture; xfli@mail.csu.edu.cn (Corresponding Author).

$\nu(r)$ at the interface of a multilayered structure. Such a jump in σ_θ can be avoided when discontinuous material properties are taken as continuously varying material properties.

Next, putting Eq. (5) into Eq. (7) then into Eq. (2), we get an integro-differential equation as follows:

$$\frac{\mathrm{d}\sigma_r}{\mathrm{d}r}+\frac{2[1-2\nu(r)]}{r[1-\nu(r)]}\sigma_r-\frac{2E(r)}{r^2\chi(r)[1-\nu(r)]}\times\left[A+\int_{r_0}^{r}\frac{[1+\nu(s)][1-2\nu(s)]\chi(s)}{[1-\nu(s)]E(s)}\sigma_r(s)\,\mathrm{d}s\right]=0 \tag{8}$$

Furthermore, by integrating both sides of the preceding equation with respect to r, one can get

$$\sigma_r+\int_{r_0}^{r}K(r,\rho)\sigma_r(\rho)\,\mathrm{d}\rho=B+Af(r) \tag{9}$$

with

$$K(r,\rho)=\frac{2[1-2\nu(\rho)]}{\rho[1-\nu(\rho)]}-\frac{[1+\nu(\rho)][1-2\nu(\rho)]\chi(\rho)}{[1-\nu(\rho)]E(\rho)}\times\int_{\rho}^{r}\frac{2E(s)}{s^2\chi(s)[1-\nu(s)]}\,\mathrm{d}s$$
$$f(r)=\int_{r_0}^{r}\frac{2E(s)}{s^2\chi(s)[1-\nu(s)]}\,\mathrm{d}s \tag{10}$$

where $K(r,\rho)$ and $f(r)$ in Eq. (9) are known, and A and B are two unknown constants.

Furthermore, when considering a pressurized FGM hollow sphere with the inner and outer radii, a and b, respectively, the corresponding boundary conditions can be stated as $\sigma_r(a)=-q_i$ and $\sigma_r(b)=-q_o$, where q_i and q_o are two constants. Using these two conditions, A and B in Eq. (9) can be determined. Knowledge of A and B allows us to further rewrite Eq. (9) as the following form:

$$\sigma_r(r)+\int_{a}^{b}L(r,\rho)\sigma_r(\rho)\,\mathrm{d}\rho=h(r) \tag{11}$$

where $h(r)=-q_i-(q_o-q_i)f(r)/f(b)$ and

$$L(r,\rho)=\begin{cases}K(r,\rho)-\frac{f(r)}{f(b)}K(b,\rho), & \rho<r,\\ -\frac{f(r)}{f(b)}K(b,\rho), & \rho>r\end{cases} \tag{12}$$

III. Spherically Transversely Isotropic FGM Spheres

The results derived in the preceding can be directly extended to a spherically transversely isotropic FGM hollow sphere. For this purpose, keeping in mind that the equilibrium equation (2) remains unchanged, the only difference is that the following stress–strain relations for a spherically transversely isotropic material,

$$\frac{\mathrm{d}u_r}{\mathrm{d}r}=\frac{1}{E}(\sigma_r-2\nu\sigma_\theta),\qquad \frac{u_r}{r}=\frac{1-\nu}{E^*}\sigma_\theta-\frac{\nu}{E}\sigma_r \tag{13}$$

are used instead of those in Eq. (1).

Following the same procedure as the preceding, we have

$$\sigma_r=\frac{E(r)}{\lambda(r)-2\nu^2(r)}\left[\lambda(r)\frac{\mathrm{d}u_r}{\mathrm{d}r}+2\nu(r)\frac{u_r}{r}\right]$$
$$\sigma_\theta=\frac{E(r)}{\lambda(r)-2\nu^2(r)}\left[\frac{u_r}{r}+\nu(r)\frac{\mathrm{d}u_r}{\mathrm{d}r}\right] \tag{14}$$

where $\lambda(r)=[1-\nu(r)]E(r)/E^*(r)$. Then we represent

$$u_r(r)=\frac{1}{\chi(r)}\left[A+\int_{r_0}^{r}\frac{[\lambda(s)-2\nu^2(s)]\chi(s)}{\lambda(s)E(s)}\sigma_r(s)\,\mathrm{d}s\right] \tag{15}$$

with

$$\chi(r)=\exp\left[\int_{r_0}^{r}\frac{2}{s}\left(1-\frac{\nu(s)E^*(s)}{[1-\nu(s)]E(s)}\right)\mathrm{d}s\right]$$

In this case, the following integral equation can be derived:

$$\sigma_r+\int_{r_0}^{r}K(r,\rho)\sigma_r(\rho)\mathrm{d}\rho=B+Af(r) \tag{16}$$

with

$$K(r,\rho)=\frac{2}{\rho}\left(1-\frac{\nu(\rho)E^*(\rho)}{[1-\nu(\rho)]E(\rho)}\right)-\frac{[\lambda(\rho)-2\nu^2(\rho)]\chi(\rho)}{\lambda(\rho)E(\rho)}\times\int_{\rho}^{r}\frac{2E^*(s)}{s^2\chi(s)[1-\nu(s)]}\,\mathrm{d}s$$
$$f(r)=\int_{r_0}^{r}\frac{2E^*(s)}{s^2\chi(s)[1-\nu(s)]}\,\mathrm{d}s \tag{17}$$

IV. Numerical Results and Discussions

Defining normalized variables x and t such that $r=(b+a)/2+(b-a)x/2$ and $\rho=(b+a)/2+(b-a)t/2$, Eq. (11) can be rewritten as

$$\sigma(x)+\int_{-1}^{1}F(x,t)\sigma(t)\,\mathrm{d}t=g(x) \tag{18}$$

where $\sigma(x)=\sigma_r(r)$, $g(x)=h(r)$, and $F(x,t)=(b-a)L(r,\rho)/2$.

In what follows, we invoke the Legendre polynomial method to determine the numerical solution to Eq. (18). Rather, $\sigma(x)$ can be approximately expanded as

$$\sigma(x)=\sum_{n=0}^{N}c_nP_n(x),\qquad -1\le x\le 1 \tag{19}$$

where $P_n(x)$ are Legendre polynomials, c_n are unknown coefficients, and the first $N+1$ terms are chosen, due to a negligible contribution of the rest. It is easily shown that c_n can be determined by solving a system of linear algebraic equations [13]:

$$\frac{2}{2m+1}c_m+\sum_{n=0}^{N}l_{mn}c_n=g_m,\qquad m=0,1,2,\ldots,N \tag{20}$$

with

$$l_{mn}=\int_{-1}^{1}\int_{-1}^{1}P_m(x)F(x,t)P_n(t)\,\mathrm{d}t\,\mathrm{d}x$$
$$g_m=\int_{-1}^{1}P_m(x)g(x)\,\mathrm{d}x$$

Therefore, the distribution of the radial stress component $\sigma_r(r)=\sigma(x)$ can be evaluated from Eq. (19). Furthermore, u_r and σ_θ are also obtainable. For a spherically transversely isotropic hollow sphere, u_r and σ_θ are also calculated via a similar procedure.

For most materials, Poisson's ratio is nearly a constant, and so in the following calculations, we only consider arbitrary radial nonhomogeneity of Young's modulus. However, it is noted that varying Poisson's ratio can be similarly solved, which does not bring any further difficulty. To check the accuracy of the present method, we consider a special Young's modulus with power-law form: that is,

$$E(r)=E_i\left(\frac{r}{a}\right)^{\beta},\qquad \nu(r)=\nu \tag{21}$$

where E_i is Young's modulus at the inner surface material. For this case, the exact stress distribution induced by internally uniform pressure $-q_i$ and $q_o=0$ is [6]

$$\sigma_r(r)=-q_i\left(\frac{a}{r}\right)^{(3+k-\beta)/2}\frac{b^k-r^k}{b^k-a^k} \tag{22}$$

$$\sigma_\theta(r) = q_i\left(\frac{a}{r}\right)^{(3+k-\beta)/2}\frac{1}{b^k-a^k}\left[\frac{2-(1+\beta+k)\nu}{(1-\nu)(1+\beta+k)-4\nu}b^k - \frac{2-(1+\beta-k)\nu}{(1-\nu)(1+\beta-k)-4\nu}r^k\right] \tag{23}$$

where $k=\sqrt{(1+\beta)^2+8-8\beta\nu/(1-\nu)}$.

Numerical results are evaluated for several different values of β for $a/b=0.6$ and $\nu=0.3$, and Fig. 1 shows the distribution of $\sigma_r(r)/q_i$ and $\sigma_\theta(r)/q_i$. We find that by taking only the first four terms of Legendre polynomials ($N=3$), the obtained results are rather satisfactory. From Fig. 1, it is seen that the numerical results are quite accurate, and so the suggested method is very efficient. Note that the exact solution given by Eqs. (22) and (23) only applies to Young's modulus of power-law nonhomogeneity. For a general case, the preceding exact solution fails. Nevertheless, our approach can tackle arbitrarily varying elastic modulus. Here, we consider a typical variation of Young's modulus [14]:

$$E(r) = E_i\left[1+(\alpha-1)\left(\frac{r-a}{b-a}\right)^\beta\right] \tag{24}$$

where α denotes the ratio of Young's modulus at the outer surface to that at the inner surface. From the preceding, with an increase in r, $E(r)$ is monotonically increasing if $\alpha>1$ and monotonically decreasing if $\alpha<1$, which means that the hollow sphere becomes stiffer if $\alpha>1$ or more compliant if $\alpha<1$ when r rises. In addition, the gradient index β represents that the curve of $E(r)$ is concave if $\beta>1$ and convex if $\beta<1$. Particularly, $E(r)$ is a linear function of r if $\beta=1$.

The effects of α on the stress distribution are examined for a linearly varying Young's modulus. The response of the radial and hoop stresses is presented in Fig. 2. From Fig. 2a, $\sigma_r(r)$ is compressive and monotonically increases from $-p$ at the inner surface to zero at the outer surface, regardless of the values of α. Compared with $\sigma_r(r)$, the effects of α on $\sigma_\theta(r)$ are pronounced. In the FGM hollow

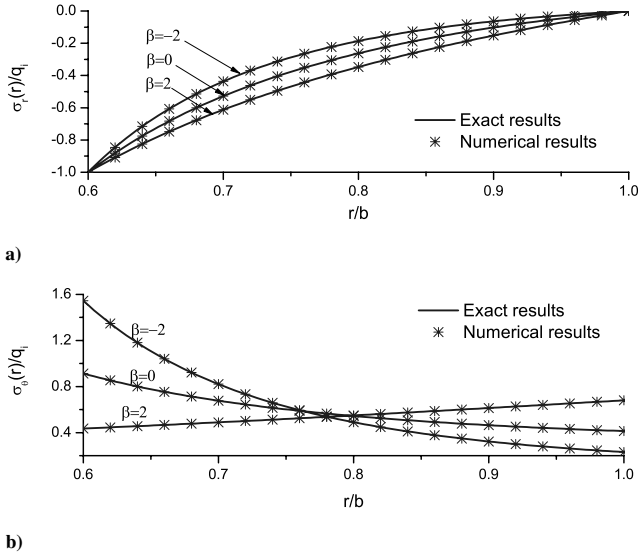

Fig. 1 Stress distribution in an internally pressurized FGM hollow sphere with $a/b=0.6$, $\nu=0.3$, and $E(r)$ given by Eq. (21); exact results (solid lines) and numerical results with $N=3$ (asterisks): a) radial stress $\sigma_r(r)/q_i$ and b) hoop stress $\sigma_\theta(r)/q_i$.

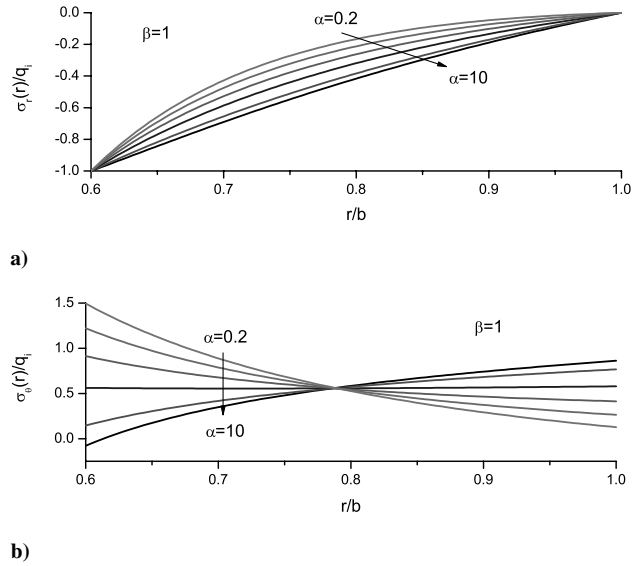

Fig. 2 Effects of the parameter α on the stress distribution for a linearly varying Young's modulus [Eq. (24)] at $\alpha=0.2, 0.5, 1, 2$, and 10: a) radial stress $\sigma_r(r)/q_i$ and b) hoop stress $\sigma_\theta(r)/q_i$.

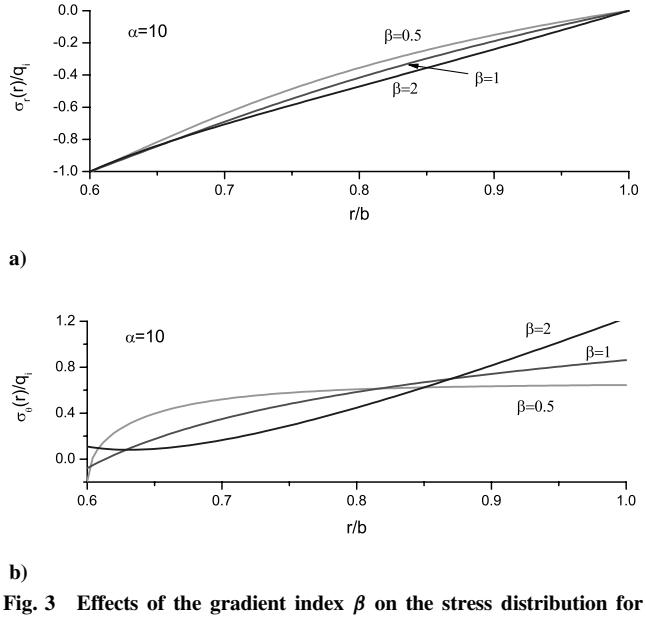

Fig. 3 Effects of the gradient index β on the stress distribution for Young's modulus of form of Eq. (24) at $\alpha=10$: a) radial stress $\sigma_r(r)/q_i$ and b) hoop stress $\sigma_\theta(r)/q_i$.

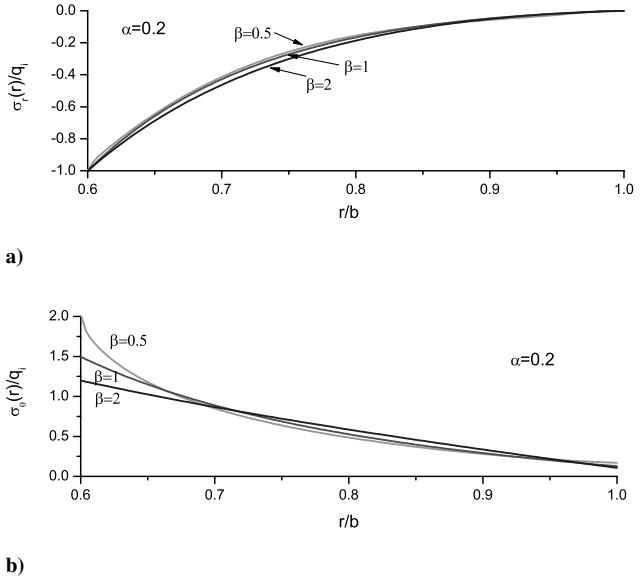

Fig. 4 Effects of the gradient index β on the stress distribution for Young's modulus of form of Eq. (24) at $\alpha=0.2$: a) radial stress $\sigma_r(r)/q_i$ and b) hoop stress $\sigma_\theta(r)/q_i$.

sphere, $\sigma_\theta(r)$ reaches its maximum tensile stress at the inner surface, then progressively drops when r rises and finally reaches its minimum stress at the outer surface for α, taking smaller values such as $\alpha = 0.2$, 0.5, and 1. When α takes larger values ($\alpha = 5$, 10), the preceding trend is reversed. That is, σ_θ goes from its minimum value at the inner surface to its maximum value at the outer surface. In particular, when α takes a value near 2, σ_θ is almost unchanged. Such a characteristic is useful for optimal design of an FGM hollow sphere in engineering applications, because most failure of this spherical structure results from the hoop stress exceeding its critical value. A preferable β value is to causes the hoop stress to reach its critical value almost simultaneously.

Figures 3 and 4 are devoted to the effects of the gradient index β on the stress distribution. For σ_r, the trend is similar, whereas for σ_θ, the influence of β is completely different. For instance, when $\alpha = 10$, $\sigma_\theta(r)$ (as seen in Fig. 3b) has a minimum value at an internal position rather than at the surfaces for $\beta = 2$. Additionally, the maximum value of σ_θ is clearly reduced for $\beta = 0.5$. For this case, the hoop stress has a dramatic variation near the inner surface ($r/b < 0.7$), and then it almost exhibits a platform when $r/b > 0.7$. As a result, if two surface materials are given, we can choose a suitable gradient index β such that the variation of σ_θ is slight. Another interesting point is that the effects of the gradient index β are also dependent on the value of α, which can be observed by comparing Fig. 3 for $\alpha = 10$ with Fig. 4 for $\alpha = 0.2$.

V. Conclusions

The spherical symmetrical problem of FGM spheres is studied. This paper reduces the problem to a Fredholm integral equation. This method does not require any limitation on the material properties and applies to an arbitrarily varying Young's modulus and Poisson's ratio. Solving the resulting equation, the distribution of the stress components is obtainable. For a typically varying Young's modulus, numerical results of the radial and hoop stresses are evaluated and presented graphically. Our results indicate that change in the gradient of the FGM sphere does not produce a substantial variation of the radial stress, but strongly affects the hoop stress. The obtained results are helpful in designing FGM vessels for the purpose of structural integrity.

Acknowledgment

This work was supported by the National Natural Science Foundation of China under Grant no. 10672189.

References

[1] Timoshenko, S. P., and Goodier, J. N., "Theory of Elasticity," 3rd ed., McGraw–Hill, New York, 1970.

[2] Bufler, H., "The Arbitrarily and the Periodically Laminated Elastic Hollow Sphere: Exact Solutions and Homogenization," *Archive of Applied Mechanics*, Vol. 68, No. 9, 1998, pp. 579–588. doi:10.1007/s004190050188

[3] Heyliger, P., and Wu, Y. C., "Electroelastic Fields in Layered Piezoelectric Spheres," *International Journal of Engineering Science*, Vol. 37, No. 2, 1999, pp. 143–161. doi:10.1016/S0020-7225(98)00068-8

[4] Chen, W. Q., and Ding, H. J., "A State-Space-Based Stress Analysis of a Multilayered Spherical Shell with Spherical Isotropy," *Journal of Applied Mechanics*, Vol. 68, No. 1, 2001, pp. 109–114. doi:10.1115/1.1343913

[5] Olsson, M., Giannakopoulos, A. E., and Suresh, S., "Elastoplastic Analysis of Thermal Cycling: Ceramic Particles in a Metallic Matrix," *Journal of the Mechanics and Physics of Solids*, Vol. 43, No. 10, 1995, pp. 1639–1671. doi:10.1016/0022-5096(95)00046-L

[6] Tutuncu, N., and Ozturk, M., "Exact Solutions for Stresses in Functionally Graded Pressure Vessels," *Composites, Part B*, Vol. 32, No. 8, 2001, pp. 683–686. doi:10.1016/S1359-8368(01)00041-5

[7] Eslami, M. R., Babaei, M. H., and Poultangari, R., "Thermal and Mechanical Stresses in a Functionally Graded Thick Sphere," *International Journal of Pressure Vessels and Piping*, Vol. 82, No. 7, 2005, pp. 522–527. doi:10.1016/j.ijpvp.2005.01.002

[8] Poultangari, R., Jabbari, M., and Eslami, M. R., "Functionally Graded Hollow Spheres Under Non-Axisymmetric Thermo-Mechanical Loads," *International Journal of Pressure Vessels and Piping*, Vol. 85, No. 5, 2008, pp. 295–305. doi:10.1016/j.ijpvp.2008.01.002

[9] Chen, W. Q., "Stress Distribution in a Rotating Elastic Functionally Graded Material Hollow Sphere with Spherical Isotropy," *Journal of Strain Analysis for Engineering Design*, Vol. 35, No. 1, 2000, pp. 13–20.

[10] You, L. H., Zhang, J. J., and You, X. Y., "Elastic Analysis of Internally Pressurized Thick-Walled Spherical Pressure Vessels of Functionally Graded Materials," *International Journal of Pressure Vessels and Piping*, Vol. 82, No. 5, 2005, pp. 347–354. doi:10.1016/j.ijpvp.2004.11.001

[11] Guven, U., and Baykara, C., "On Stress Distributions in Functionally Graded Isotropic Spheres Subjected to Internal Pressure," *Mechanics Research Communications*, Vol. 28, No. 3, 2001, pp. 277–281. doi:10.1016/S0093-6413(01)00174-4

[12] Batra, R. C., "Optimal Design of Functionally Graded Incompressible Linear Elastic Cylinders and Spheres," *AIAA Journal*, Vol. 46, No. 8, 2008, pp. 2050–2057. doi:10.2514/1.34937

[13] Li, X.-F., and Peng, X.-L., "A Pressurized Functionally Graded Hollow Cylinder with Arbitrarily Varying Material Properties," *Journal of Elasticity*, Vol. 96, No. 1, 2009, pp. 81–95. doi:10.1007/s10659-009-9199-z

[14] Li, X.-F., "A Unified Approach for Analyzing Static and Dynamic Behaviors of Functionally Graded Timoshenko and Euler-Bernoulli Beams," *Journal of Sound and Vibration*, Vol. 318, Nos. 4–5, 2008, pp. 1210–1229. doi:10.1016/j.jsv.2008.04.056

F. Pai
Associate Editor